Atomic layer deposition-SiO$_2$ layers protected PdCoNi nanoparticles supported on TiO$_2$ nanopowders: Exceptionally stable nanocatalyst for the dehydrogenation of formic acid

Nurdan Caner[a], Ahmet Bulut[a], Mehmet Yurderi[a], Ilknur Efecan Ertas[a], Hilal Kivrak[b], Murat Kaya[c], Mehmet Zahmakiran[a],*,[1]

[a] *Nanomaterials and Catalysis (NanoMatCat) Research Laboratory, Department of Chemistry, Yuzuncu Yil University, 65080, Van, Turkey*
[b] *Department of Chemical Engineering Yuzuncu Yıl University, 65080, Van, Turkey*
[c] *Department of Chemical Engineering and Applied Chemistry, Atilim University, 06836, Ankara, Turkey*

ARTICLE INFO

ABSTRACT

TiO$_2$ nanopowders supported trimetallic PdCoNi alloy nanoparticles were simply and reproducibly prepared by wet-impregnation followed by simultaneous reduction method, then to enhance their stability against to sintering and leaching atomic layer deposition (ALD) technique was utilized to grow SiO$_2$ layers amongst these surface bound PdCoNi alloy nanoparticles (PdCoNi/TiO$_2$-ALD-SiO$_2$). These new nanomaterials are characterized by the combination of complimentary techniques and sum of their results exhibited that the formation of ALD-SiO$_2$ layers protected well-dispersed and highly crystalline PdCoNi alloy nanoparticles (ca. 3.52 nm) supported on TiO$_2$ nanopowders. The catalytic performance of the resulting PdCoNi/TiO$_2$-ALD-SiO$_2$ in terms of activity, selectivity and stability was investigated in the dehydrogenation of aqueous formic acid (HCOOH), which has recently been suggested as a promising hydrogen storage material with a 4.4 wt% hydrogen capacity, solution under mild conditions. The results collected from our systematic studies revealed that PdCoNi/TiO$_2$-ALD-SiO$_2$ nanomaterial can act as highly active and selective nanocatalyst in the formic acid dehydrogenation at room temperature by providing an *initial* turnover frequency (TOF) value of 207 mol H$_2$/mol metal × h and >99% of dehydrogenation selectivity at almost complete conversion. More importantly, the catalytic reusability experiments separately carried out with PdCoNi/TiO$_2$-ALD-SiO$_2$ and PdCoNi/TiO$_2$ nanocatalysts in the dehydrogenation of formic acid under more forcing conditions pointed out that PdCoNi/TiO$_2$-ALD-SiO$_2$ nanocatalyst displays unprecedented catalytic stability against to leaching and sintering throughout the reusability experiments it retains almost its inherent activity, selectivity and conversion even at 20th reuse, whereas analogous PdCoNi/TiO$_2$ completely lost its catalytic performance.

© 2017 Elsevier B.V. All rights reserved.

1. Introduction

Catalysis has received a tremendous amount of interest, both from a scientific and an industrial perspective and has an enormous impact on the world economy, since more than 95% of chemical manufacturing processes utilize catalysts [1]. Particularly, one area of catalysis that is developing at a rapid pace is nanocatalysis; striking novel catalytic properties including greatly enhanced reactivities and selectivities have been reported for nanoparticles (NPs) catalysts as compared to their bulk counterparts [2]. Among,

various types of nanocatalysts, transition metal NPs on oxide supports represent the most important group of nanocatalysts [3], because of their advantages in application such as simple synthesis routes and isolation procedures [4]. Additionally, supported metal NPs usually provide kinetic control of catalytic reactions [5], which is very tricky in the case of support-free colloidal metal NPs in "semi-homogeneous" catalysis [6]. Today, a challenging issue in the fabrication of supported metal NPs is the achievement of highly stable, compositionally well-defined, shape- and size-controllable NPs. When the reaction is structure sensitive, the catalytic activity of metal NPs is drastically influenced by their size as they control the surface structure, electronic and oxidation states. Improving the stability of supported metal NPs against sintering and leaching under reaction conditions has also drawn a lot of attention,

---

* Corresponding author.
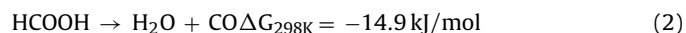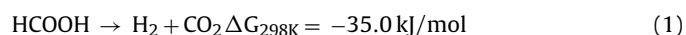 *E-mail address:* zmehmet@yyu.edu.tr (M. Zahmakiran).
[1] www.nanomatcat.com.

especially for catalytic reactions that require harsh reaction conditions, since the sintering and/or leaching of surface bound metal NPs leads to a momentous decrease in their catalytic activity and lifetime [2–5].

In this context, various methods have been developed to encapsulate noble metal NPs in various types of porous materials using techniques such as grafting, chemical vapor deposition (CVD), dendrimer encapsulation, micro-emulsion, etc. to form core-protective shell structures [7–12]. Although, some of these protective shell encapsulated metal NPs have showed good sintering resistance up to 800 °C, in most cases a large decrease in catalytic activity has been observed due to mass transfer limitations connected with the protective shell. At this concern, a method which allows atomically precise control over the thickness and composition of protective layers can preserve catalytic activity of supported metal NPs to the greatest extent while improving their stability.

Atomic layer deposition (ALD) is a thin film growth technique similar to CVD, except that the deposition is broken down into cycles each of which is a sequence of two surface reactions [13] and in contrast to previous surface coating techniques ALD provides the possibility for atomically controlled post-modification of supported metal NPs by applying protective over-coats [14]. More importantly, the self-limiting, layer-by-layer deposition feature of ALD enables us to precisely control over the thickness of the protective layer, which protects surface supported metal NPs against to sintering and leaching, therefore it is a most promising way of solving the mass transfer resistance problem. For example, Stair et al. [15] showed that ALD Al_2O_3 over-coats effectively prevent sintering of Al_2O_3 supported Pd NPs up to 500 °C without decreasing their inherent activity. In another more recent study, Stair and co-workers have developed a new methodology to protect supported metal NPs against to sintering and leaching [16]. This new method involves growing uniform, dispersed Pd NPs, protecting the particles with a blocking agent, growing a metal oxide structure around the nanoparticle using ALD, and removing the blocking agent. The resulting ALD oxide created "nanobowls" prevented the sintering of Pd nanoparticles throughout the repatitive calcination-reduction steps performed at elevated temperatures (>300 °C). The excellent stability performances obtained from these studies prompted us to utilize ALD technique to prepare highly stable solid oxide supported metal NPs for the dehydrogenation of formic acid.

Of particular importance, formic acid (FA, HCOOH), which is one of the major products formed in biomass processing and also accessible via variety of processes such as hydrolysis of methyl formate or CO_2 hydrogenation [17,18], has recently been suggested as the promising hydrogen storage material due to its high energy density, stability and nontoxicity [19,20]. In general, FA can be decomposed via dehydrogenation (1) and dehydration (2) pathways depending on the catalyst, pH of the medium and the reaction temperature [20].

$$HCOOH \rightarrow H_2 + CO_2 \quad \Delta G_{298K} = -35.0 \, kJ/mol \qquad (1)$$

$$HCOOH \rightarrow H_2O + CO \quad \Delta G_{298K} = -14.9 \, kJ/mol \qquad (2)$$

The selective dehydrogenation of FA is crucial for the production of ultrapure H_2, since toxic carbon monoxide (CO) contamination produced by the dehydration pathway significantly reduces the activity of Pt catalysts used in proton exchange membrane fuel cells (PEMFC) [21]. Recently, serious labors have been conducted on the development of active and selective homogeneous catalysts for FA dehydrogenation [22,23]. Notwithstanding, prominent catalytic performances have been achieved in some of these catalysts [24,25] the significant challenges linked with the recovery and reusability significantly hinder the practical use of such catalytic systems for on-board applications. In this context, the majority of the recent studies have been focused on the development of palladium (Pd),

which known as the most active noble metal in FA dehydrogenation, based solid supported metal nanoparticles catalysts [26–40] exhibiting significant activity under mild conditions with high selectivity and facile catalyst recovery capabilities. Despite these plentiful former efforts, the plurality of these reported heterogeneous catalysts require elevated temperatures [41–43], while revealing low activity and reusability performances.

The low reusability performance of these systems mainly associated with the sintering and leaching of active metal NPs supported on solid materials that cling to the surface of the support material via weak physical adsorption. On the other hand, the main reason of the low catalytic performances obtained by these Pd based catalytic systems is the ease poisoning of active Pd centers by CO, which can form as intermediate in both dehydrogenation and dehydration pathways of FA decomposition [19,20]. At this concern, alloying with another metal that has better CO anti-poisoning ability over Pd, seems to be promising way to prevent CO-deactivation of Pd [29–40]. In addition to enhancement of CO poisoning resistivity, alloying of Pd with another metal especially first-row metals also reduce the consumption of high-cost Pd. Thus, it is highly fascinating to further increase CO resistance, catalytic performance of Pd NPs and lower the cost of nanocatalyst by integration of low-cost metals.

Taking all these problems into consideration, herein we report a successful attempt at the ALD-SiO_2 layers protected PdCoNi alloy NPs supported on TiO_2 nanopowders, hereafter referred to as PdCoNi/TiO_2-ALD-SiO_2, through a synthesis route that involves (*i*) the preparation of TiO_2 nanopowders supported PdCoNi alloys NPs by the conventional wet-impregnation followed by simultaneous reduction method, (*ii*) the protecting of PdCoNi NPs surface with oleylamine (OAm; $CH_3(CH_2)_7CH=CH(CH_2)_7CH_2NH_2$), which acted as a blocking agent to prevent growing of SiO_2 layers on PdCoNi NPs, (*iii*) the growing of SiO_2 layer around surface-protected PdCoNi alloy NPs to optimum thickness for catalysis and then (*iv*) removing blocking agent through acetic acid washing-calcination-H_2 reduction steps. The resulting PdCoNi/TiO_2 and PdCoNi/TiO_2-ALD-SiO_2 nanocatalysts were characterized by using advanced analytical techniques and their catalytic performances in terms of catalytic activity, selectivity and stability were investigated in the dehydrogenation of aqueous FA solution under mild conditions. We found that PdCoNi/TiO_2-ALD-SiO_2 nanocatalyst catalyzes the dehydrogenation of aqueous FA solution with an *initial* turnover frequency (TOF) value of 207 mol H_2/mol metal × h at >99% of dehydrogenation selectivity and almost complete conversion ($\geq$92%). Moreover, PdCoNi/TiO_2-ALD-SiO_2 nanocatalyst exhibits excellent catalytic stability against to leaching and sintering throughout the reusability experiments performed in FA dehydrogenation at elevated temperature; it retains almost its inherent activity and selectivity even at 20th reuse, whereas ALD-SiO_2 unprotected TiO_2 supported PdCoNi (PdCoNi/TiO_2) NPs completely lost their catalytic performance due to their sintering on TiO_2 surface under the same reaction conditions.

2. Experimental

2.1. Materials

Palladium(II) nitrate dihydrate (Pd(NO$_3$)$_2$·2H$_2$O), cobalt(II) chloride hexahydrate (CoCl$_2$·6H$_2$O), nickel(II) chloride trihydrate (NiCl$_2$·6H$_2$O), sodium borohydride (NaBH$_4$), 3-aminopropyltriethoxysilane (H$_2$N(CH$_2$)$_3$Si(OC$_2$H$_5$)$_3$, APTS), oleylamine (CH$_3$(CH$_2$)$_7$CH=CH(CH$_2$)$_7$CH$_2$NH$_2$, OAm), titania nanopowders (TiO$_2$) and sodium hydroxide (NaOH) were purchased from Sigma-Aldrich®. Formic acid (FA; CH$_2$O$_2$, >96%), and sodium formate (SF; HCOONa) were purchased from Merck®.

High purity of H_2 (99.9%) and Ar (99.9%) were purchased from Linde-Gas and used as received. Deionized water was distilled by water purification system (Milli-Q Water Purification System). All glassware and teflon-coated magnetic stirring bars were washed with acetone and copiously rinsed with distilled water before drying in an oven at 150 °C.

2.2. Characterization

Palladium, nickel and cobalt contents of the samples was determined by inductively coupled plasma optical emission spectroscopy (ICP-OES; Leeman, Direct Reading Echelle) after each sample was completely dissolved in a mixture of HNO_3/HCl (1/3 ratio). Bright field transmission electron microscopy (BFTEM) samples were prepared by dropping one drop of dilute suspension on copper coated carbon BFTEM grid and the solvent was then dried. The BFTEM was carried out on a JEOL JEM-200CX transmission electron microscopes operating at 120 kV. High resolution transmission electron microscopy (HRTEM), scanning transmission electron microscopy (STEM), and high angle annular dark field scanning transmission electron microscopy (HAADF-STEM) were run on a JEOL JEM-2010F transmission electron microscope operating at 200 kV. Oxford energy dispersive X-ray (EDX) system and Inca software were used to collect and process STEM-EDX data. High resolution X-ray photoelectron spectroscopy (HR-XPS) analyses were performed on a Physical Electronics 5800-spectrometer equipped with a hemispherical analyzer and using monochromatic Al-Kα radiation (1486.6 eV, the X-ray tube working at 15 kV and 350 W, and pass energy of 23.5 eV). Gas phase decomposition products of FA were analyzed by gas chromatography (GC) using FID-2014 and TCD-2014 GC analyzers (Shimadzu) and FTIR spectroscopy (Shimadzu IR-Affinity).

2.3. Preparation of PdCoNi alloy nanoparticles supported on TiO$_2$ nanopowders

PdCoNi/TiO$_2$ nanocatalyst was obtained by the conventional impregnation and subsequent reduction steps. Typically, 5.0 mL aqueous solution containing Pd(NO$_3$)$\cdot$2H$_2$O (13.35 mg, 50.0 μmol Pd), CoCl$_2$·6H$_2$O (3.33 mg, 14.0 μmol Co), NiCl$_2$·6H$_2$O (3.54 mg, 15.0 μmol Ni) and TiO$_2$ nanopowders (140 mg) is mixed for 3 h. Then, the fresh 1.0 mL aqueous solution of NaBH$_4$ (47.4 mg, 11.85 mmol) was added to this mixture and the resulting solution was stirred for half an hour under ambient conditions. After centrifugation (6000 rpm, 5 min), copious washing with water (3 × 20 mL), filtration, and drying in oven at 100 °C, PdCoNi/TiO$_2$ nanocatalyst was obtained as a dark gray powder.

2.4. Atomic layer deposition of SiO$_2$ (ALD-SiO$_2$) protecting layers on PdCoNi/TiO$_2$

Before performing ALD-SiO$_2$ deposition on PdCoNi/TiO$_2$, the surface protection of PdCoNi NPs was done by using oleylamine (OAm; CH$_3$(CH$_2$)$_7$CH=CH(CH$_2$)$_7$CH$_2$NH$_2$) as blocking agent. For this purpose, PdCoNi/TiO$_2$ nanocatalyst was immersed into 20.0 mL hexane solution of OAm (10.0 mM) and mixed at 600 rpm for 12 h at room temperature. Then, the solid remnant was isolated by suction filtration using Whatman-5 filter paper, washed three times with 20.0 mL of hexane and dried in vacuum-oven at 80 °C and 10^{-1} Torr. The flow type ALD reactor (**Fig. S1**, Supporting Information) was used for ALD-SiO$_2$ deposition. Prior to the deposition, PdCoNi/TiO$_2$ was pretreated in an ALD reactor at 150–180 °C in order to remove physically adsorbed water molecules from TiO$_2$ surface. The pressure in the ALD reactor was adjusted to 20–50 mbar. Ultra high purity argon (Linde-Gas, 99.99%) was used as the carrier gas. The ALD timing sequences can be expressed as t_1–t_2–t_3–t_4, where t_1

and t_3 are the APTS precursor and water vapor exposure times, respectively and t_2 and t_4 are the argon purge times following the precursor exposures and all times are in seconds. APTS was heated to 110 °C in a stainless steel bubbler then given to system for 10 s (t_1 = 10 s). Water vapor was given into ALD reactor at 150 °C for 10 s (t_3 = 10 s). For the removal of unreacted reactants, each reaction step was followed by an argon purge (t_2 = t_4 = 10 s) at the reaction temperature. These four steps were referred to as one cycle and the over-coated samples were prepared using 1, 2, 4, 6, 10 and 20 cycles of SiO$_2$ ALD to create the protective layers. Next, in order to remove OAm blocking agents from the surface of PdCoNi NPs, PdCoNi/TiO$_2$-ALD-SiO$_2$ powders was immersed into 20.0 mL acetone/acetic acid (v/v = 1/1) and stirred in this mixture for 12 h at room temperature [33,34]. Then, the solid PdCoNi/TiO$_2$-ALD-SiO$_2$ powders was isolated by suction filtration using Whatman-5 filter paper, and dried in vacuum-oven at 80 °C and 10^{-1} Torr. Finally, PdCoNi/TiO$_2$-ALD-SiO$_2$ powders was firstly taken into U-tube oven and sputtered with O$_2$ at 500 °C for 2 h, then room temperature cooled sample of PdCoNi/TiO$_2$-ALD-SiO$_2$ was reduced with H$_2$ at 200 °C for 4 h in U-tube oven. The resulting PdCoNi/TiO$_2$-ALD-SiO$_2$ powders was cooled to room temperature and taken into Labsconco nitrogen-atmosphere glovebox (H$_2$O < 3 ppm, O$_2$ < 1 ppm).

2.5. Measurement of catalytic activity in dehydrogenation of aqueous formic acid solution

The catalytic activity of PdCoNi/TiO$_2$-ALD-SiO$_2$ in the FA dehydrogenation was determined previously established procedure that based on the volumetric measurement of the rate of hydrogen evolution. The volume of released gas during the reaction was monitored using a gas burette through water displacement as described elsewhere [26–40]. Before starting the catalytic activity tests, a jacketed one-necked reaction flask (50.0 mL) containing a teflon-coated stirring bar was placed on a magnetic stirrer (Heidolph MR-3004) whose temperature was adjusted by circulating water through its jacket from a constant temperature bath (Lab Companion RW-0525). In a typical catalytic activity test, PdCoNi/TiO$_2$-ALD-SiO$_2$ nanocatalyst was weighed and transferred into the reaction flask, and then 9.0 mL H$_2$O was added into the reaction flask followed by rigorous stirring for 15 min to achieve thermal equilibrium. Next, 1.0 mL aqueous FA solution (0.175 M FA + 0.175 M SF) was added into the reaction flask via its septum by using a 1.0 mL gastight syringe and the catalytic reaction was started (t = 0 min) by stirring the mixture at 900 rpm.

2.6. Determination of catalytic selectivity in dehydrogenation of aqueous formic acid solution

The selectivity of PdCoNi/TiO$_2$-ALD-SiO$_2$ nanocatalyst in the decomposition of FA was investigated by GC, FTIR analyses and NaOH-trap experiments. The gas generated over PdCoNi/TiO$_2$-ALD-SiO$_2$ catalyzed dehydrogenation of aqueous FA solution (0.175 M FA + 0.175 M SF) was separately collected in GC analyzing balloon and FTIR gas sample holder, which were then analyzed in GC and FTIR by using pure CO, H$_2$ and CO$_2$ as reference gases. NaOH-trap experiments were performed to determine the molar ratio of CO$_2$ to H$_2$ in the product mixture generated during the PdCoNi/TiO$_2$-ALD-SiO$_2$ catalyzed decomposition of aqueous FA solution (10.0 mL of 0.175 M FA + 0.175 M SF) [33–39]. In these experiments, the trap (10.0 M NaOH solution) was placed between the jacketed reactor and gas burette. The generated gas during the reaction was passed through the NaOH trap where CO$_2$ was captured (3). Next, the volume of the gas generated from the dehydrogenation of FA was monitored and compared to those without the trap experiment. We observed that the volume of the generated gas decreased by a factor of two in the presence of the NaOH trap. This result is indica-

tive of the complete adsorption of CO_2 in NaOH solution (3) and the presence of equivalent molar amounts of CO_2 and H_2 (1.0:1.0) in the product mixture of the PdCoNi/TiO$_2$-ALD-SiO$_2$ catalyzed FA dehydrogenation.

$$2NaOH(aq) + CO_2(g) \rightarrow Na_2CO_3(aq) + H_2O(l) \tag{3}$$
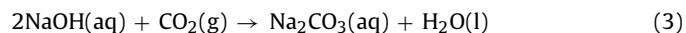
2.7. Catalytic reusability experiments in dehydrogenation of aqueous formic acid solution

The catalyst was isolated from the reaction solution by centrifugation after the first catalytic run and washed with excess water and dried at 100 °C. The dried catalyst was weighed and reused in the catalytic dehydrogenation of a 10.0 mL aqueous FA solution (0.175 M FA + 0.175 M SF) at 25 °C. The used catalyst was isolated and reused up to 20 consecutive catalytic cycles.

2.8. Cyclic voltammetry measurements

CV measurements were carried out in a conventional three-electrode cell with a Pt wire as the counter electrode and Ag/AgCl as the reference electrode with a CHI 660E potentiostat. The working electrode was a glassy carbon disk having a diameter of 3.0 mm held in a Teflon cylindrical housing. Before the CV measurements, the surface of the glassy carbon electrode was polished with alumina to prepare the surface of the electrode for the catalyst deposition process. For the electrode preparation, typically 7–9 mg of catalyst was dispersed in a 1.0 mL% 5.0 Nafion medium (Aldrich) to obtain a catalyst suspension. Then, 6.0 μL of this suspension was drop-cast on the surface of the glassy carbon electrode. Then, the electrode was dried at room temperature to remove the solvent. CV's were recorded between −0.23 and 1.0 V with a scan rate of 10 mV s^{-1} in the presence of 0.5 M H_2SO_4 and 1.0 M HCOOH. Prior to the CV experiments, the electrolyte was saturated with N_2, and the electrode surface was activated via 0.5 M H_2SO_4.

2.9. Linear sweep voltammetry (LSV) measurements

Linear sweep voltammetry (LSV) technique was employed to investigate the CO adsorption on the catalyst surface, which can poison the surface during the decomposition of FA [44,45]. Before LSV measurements, catalysts were exposed to a pretreatment process, where the catalyst surfaces were maintained at a constant potential of 0.0 V for 500 s. After the pretreatment, LSV measurements were carried out to determine the activity of the pretreated surfaces in the electrocatalytic oxidation of FA. These measurements were conducted within the bias range of −0.2 to 0.9 V in a solution containing 0.5 M H_2SO_4 and 1.0 M HCOOH using a 10 mV s^{-1} scan rate.

2.10. CO-Stripping voltammetry (LSV) measurements

CO stripping voltammetry measurements were carried out in a conventional three-electrode cell with a Pt wire as the counter electrode and Ag/AgCl as the reference electrode with a CHI 660E potentiostat. The working electrode was a glassy carbon disk having a diameter of 3.0 mm held in a Teflon cylindrical housing. 5.0 mg catalyst sample was dispersed in 1.0 mL% 5.0 Nafion® solution (Aldrich) to obtain a catalyst suspension. Next, 5.0 μL of this suspension was drop-cast on the surface of the glassy carbon electrode. All electrolyte solutions were deaerated with high-purity nitrogen for 30 min prior to the measurements. For CO stripping voltammetry, a 0.5 M H_2SO_4 solution was first bubbled with pure nitrogen for 30 min in order to remove the dissolved oxygen. CO was then purged into the solution for 20 min to allow saturation of the electrocatalyst surface with adsorbed CO, while maintaining a constant

potential of 0 0.0 V. Excess CO was then purged with nitrogen for 30 min.

3. Results and discussion

3.1. Preparation and characterization of PdCoNi alloy NPs supported on TiO$_2$ nanopowders

Trimetallic PdCoNi nanoparticles supported on titania nanopowders (PdCoNi/TiO$_2$) were simply and reproducibly prepared by wet-impregnation followed by simultaneous reduction method [4]. Typically, an aqueous solution containing palladium(II) nitrate (Pd(NO$_3$)$_2$·2H$_2$O), cobalt(II) chloride hexahydrate (CoCl$_2$·6H$_2$O), nickel(II) chloride trihydrate (NiCl$_2$·6H$_2$O) and titania nanopowders is mixed for three hours. Then, fresh NaBH$_4$ as a reducing agent was added to this mixture at which [NaBH$_4$]/[metal] ratio was kept at ∼15 to ensure complete reduction of metal ions and the resulting solution was stirred for half an hour under air at room temperature. After centrifugation, copious washing with water, and drying in oven, PdCoNi/TiO$_2$ catalyst was obtained as black powders and characterized by ICP-OES, P-XRD, HR-XPS, FE-SEM, BFTEM, HRTEM, LSV and CO-stripping voltammetry analyses.

The molar composition of the as-prepared catalyst was found to be Pd$_{0.60}$Co$_{0.18}$Ni$_{0.22}$ (1.78% wt Pd, 0.29% wt Co, and 0.36% wt Ni loadings correspond to 24.0 μmol Pd, 7.2 μmol Co and 8.8 μmol Ni) by ICP-OES analysis. P-XRD patterns of Pd$_{0.60}$Co$_{0.18}$Ni$_{0.22}$/TiO$_2$, Pd/TiO$_2$ (1.71 wt% Pd), Co/TiO$_2$ (1.62 wt% Co) and Ni/TiO$_2$ (1.66 wt% Ni) samples (**Fig. S2**, Supporting Information) did not show any Bragg peak that can be assignable to Pd, Co and Ni metals due to (*i*) the high crystallinity of TiO$_2$ support material and (*ii*) low Pd, Co and Ni loadings (<5.0 wt%). The observed Bragg peaks at 25.3, 27.5, 36.1, 37.8, 48.1, 54.0 and 55.1° can be ascribed to [101 (A)], [110 (R)], [101 (R)], [200 (R)], [200 (A)], [211 (R)] and [211 (A)], respectively reflections of Anatase (A) (JCPDS card no. 21–1272) and Rutile (R) (JCPDS card no. 88–1175) forms of TiO$_2$ nanopowders.

The oxidation states of Pd, Co and Ni in PdCoNi/TiO$_2$ sample and the changes in their binding energies with respect to Pd/TiO$_2$, Co/TiO$_2$ and Ni/TiO$_2$ samples were investigated by HR-XPS technique. The high resolution Pd 3d, Co 2p and Ni 2p XPS spectra of PdCoNi/TiO$_2$ together with their deconvoluted chemical states are given in Fig. 1, which reveal that the chemical states of Pd, Co and Ni in the PdCoNi/TiO$_2$ nanocatalyst are Pd (Pd 3d$_{5/2}$ 333.2 eV; Pd 3d$_{3/2}$ 338.4 eV), PdO (Pd 3d$_{5/2}$ 335.6 eV; Pd 3d$_{3/2}$ 340.3 eV) [35–39], Ni (Ni 2p$_{3/2}$ 858.3 eV; Ni 2p$_{1/2}$ 876.2 eV), NiO (Ni 2p$_{3/2}$ 863.8 eV; Ni 2p$_{1/2}$ 881.1 eV) [38], Co (Co 2p$_{3/2}$ 784.2 eV), CoO (Co 2p$_{3/2}$ 789.4 eV) [46]. The observation of oxide signals can be attributed to the surface oxidation of Pd, Co and Ni NPs during XPS sampling procedure [47].

HR-XPS spectroscopy was also used to understand the charge transfer tendency among Pd, Co and Ni in the PdCoNi/TiO$_2$ nanocatalyst. Pd 3d, Co 2p and Ni 2p core levels XPS spectra of Pd/TiO$_2$, Co/TiO$_2$ and Ni/TiO$_2$ samples were also given in Fig. 1. The comparison of the binding energies at Pd 3d, Co 2p and Ni 2p core levels for Pd/TiO$_2$, Co/TiO$_2$, Ni/TiO$_2$ and PdCoNi/TiO$_2$ samples uncloses that the binding energy for Pd 3d in PdCoNi/TiO$_2$ is shifted to the lower value compared with that of Pd/TiO$_2$; whereas the binding energies for Co 2p and Ni 2p are shifted to a higher value with respect to those Co/TiO$_2$ and Ni/TiO$_2$. These shifts are indicative of transfer of some electrons from Co and Ni to Pd due to (*i*) their electronegativity differences (Pd (PE) = 2.20; Co (PE) = 1.88; Ni (PE) = 1.91) [48], (*ii*) equalization of the Fermi levels owing to the difference of work functions of Pd (5.67 eV), Co (7.38 eV) and Ni (9.5 eV) [49,50]. This electron transfer in PdCoNi/TiO$_2$ points out the formation of alloy structure in trimetallic PdCoNi NPs [51] and has the potential deign
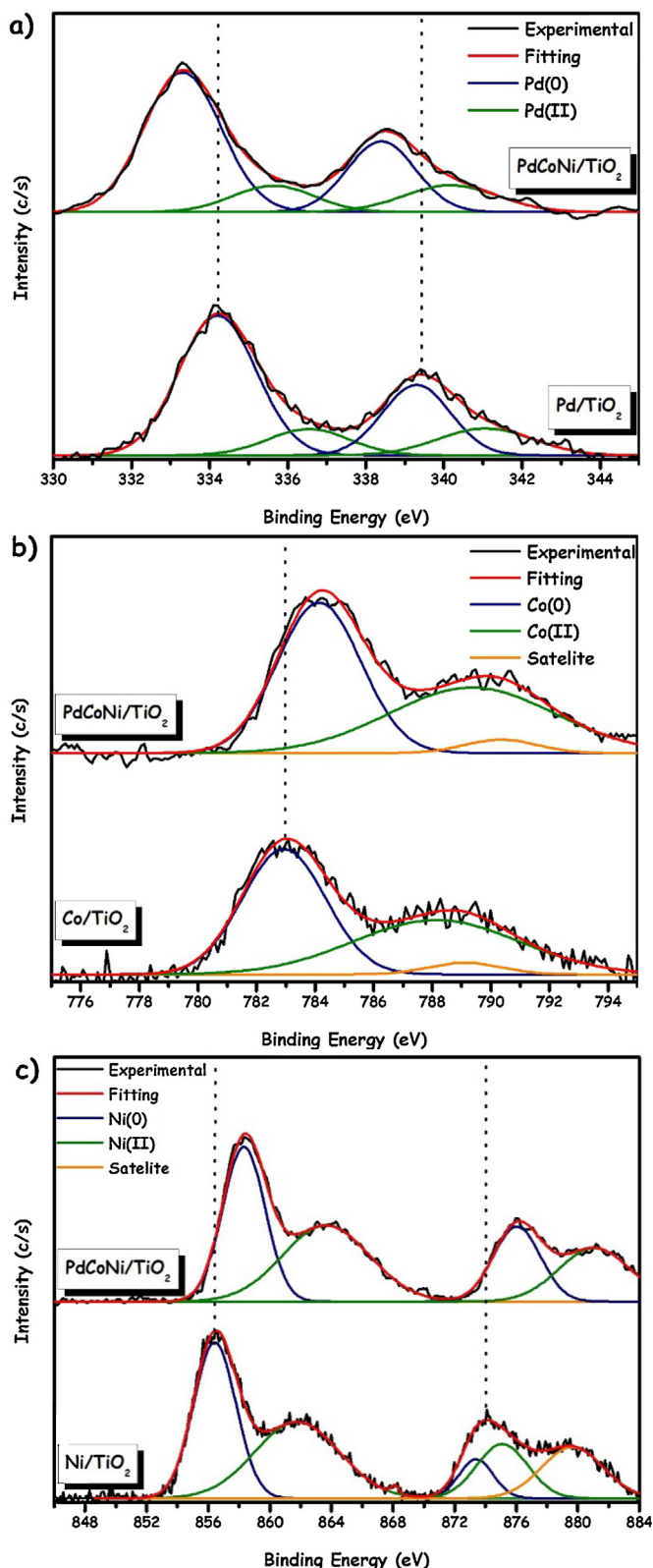
Fig. 1. High resolution Pd 3d, Co 2p and Ni 2p core levels XPS spectra with their deconvoluted chemical states of PdCoNi/TiO$_2$, Pd/TiO$_2$, Co/TiO$_2$ and Ni/TiO$_2$ samples.

itself with the high activity in FA dehydrogenation (*vide infra*) as the increase in the electron density of catalytically active Pd center facilitates metal-formate formation in the FA decomposition, which enhances the rate of the catalytic dehydrogenation of FA [52,53]. Additionally, it is well-known that the activation of transition metals deposited on TiO$_2$ is also governed cooperatively by the spin-selection rule and frontier orbital theory that emphasizes the energy gap between the frontier orbitals of transition metal and TiO$_2$ support [54]. In our case the difference between Fermi levels of TiO$_2$ [101] (7.30 eV) surface and active Pd centers (5.67 eV) most probably leads to transferring of electron density from TiO$_2$ support to active Pd centers, which also explains the high activity of PdCoNi NPs in FA dehydrogenation.

FE-SEM, BFTEM and HRTEM analyses were performed to examine the size, morphology and crystallinity of PdCoNi NPs supported on TiO$_2$ sample. FE-SEM images of PdCoNi/TiO$_2$ sample from different regions are depicted in Fig. 2(a) and (b). The inspection of these images discloses there exist only crystals of TiO$_2$ nanopowders and there is no bulk PdCoNi NPs formed in observable sizes on the surface of TiO$_2$ nanopowders. Fig. 2 also shows the BFTEM, HRTEM images and size histogram of PdCoNi/TiO$_2$ nanocatalyst. BFTEM images given in Fig. 2(c) and (d) are indicating that the formation of well-dispersed PdCoNi NPs on the surface of TiO$_2$ nanopowders, the mean diameter of the resulting PdCoNi NPs was found to be ca. 3.45 nm by using the NIH image program [55], which included the particle size analysis for >100 non-touching particles (Fig. 2(e)). It is well-known that HRTEM is a strong technique for studying alloy nanoparticles, where constituent elements lost their inherent lattice spacing and shows unique crystalline fringes in the alloy form [56]. The highly crystalline nature of the resulting PdCoNi NPs was concluded from HRTEM image of PdCoNi/TiO$_2$ nanocatalyst given in Fig. 2(f). and two distinct crystalline fringes (0.352 and 0.187 nm) were measured from this image, the crystalline fringe distance of 0.352 nm can be assignable to TiO$_2$ [101] surface [57], but the crystalline fringe distance of 0.187 nm differs from [111] spacing of the face-centered cubic (*fcc*) Pd (0.22 nm) [33], Ni (0.28 nm) [38], and Co (0.21 nm) [58] and can be ascribed to PdCoNi alloy structure [34,40,56].

3.2. Optimization of catalyst composition and effect of alloying for PdCoNi/TiO$_2$ catalyzed formic acid dehydrogenation

Before performing ALD-SiO$_2$ on PdCoNi/TiO$_2$ nanocatalyst one has to know the optimum PdCoNi composition to achieve the highest catalytic activity in FA dehydrogenation. For this reason the catalytic activities of Pd$_{0.60}$Co$_{0.18}$Ni$_{0.22}$/TiO$_2$ together with its monometallic, bimetallic and trimetallic counterparts in different molar compositions were investigated in the dehydrogenation of aqueous FA solution (0.175 M FA + 0.175 M SF) at room temperature and their results are given in Fig. 3. Obviously, Pd$_{0.60}$Co$_{0.18}$Ni$_{0.22}$/TiO$_2$ nanocatalyst provides a better activity than its mono and bimetallic counterparts prepared by the same method. From Fig. 3(a) and (b), it is clear that Pd is the needful active metal in all catalysts; without Pd addition Co$_{1.0}$/TiO$_2$, Ni$_{1.0}$/TiO$_2$ and Co$_{0.42}$Ni$_{0.58}$/TiO$_2$ catalysts show almost no catalytic reactivity. Contrariwise, the initial activity of monometallic Pd$_{1.0}$/TiO$_2$ cannot resume due to the poisoning of palladium active sites by CO formed as intermediate [19,20]. Though, bimetallic Pd$_{0.58}$Ni$_{0.42}$/TiO$_2$ and Pd$_{0.55}$Co$_{0.45}$/TiO$_2$ catalysts show better activities than Pd$_{1.0}$/TiO$_2$, their performances are still far poorer than trimetallic Pd$_{0.60}$Co$_{0.18}$Ni$_{0.22}$/TiO$_2$. The morphological investigation by BFTEM analyses (**Fig. S3**, Supporting Information) showed that mono (Pd$_{1.0}$/TiO$_2$, Co$_{1.0}$/TiO$_2$, Ni$_{1.0}$/TiO$_2$) and bimetallic (Pd$_{0.58}$Ni$_{0.42}$/TiO$_2$, Pd$_{0.55}$Co$_{0.45}$/TiO$_2$, Co$_{0.42}$Ni$_{0.58}$/TiO$_2$) catalysts have similar shapes and sizes with Pd$_{0.60}$Co$_{0.18}$Ni$_{0.22}$/TiO$_2$. The enhanced catalytic activity of Pd$_{0.60}$Co$_{0.18}$Ni$_{0.22}$/TiO$_2$ may be
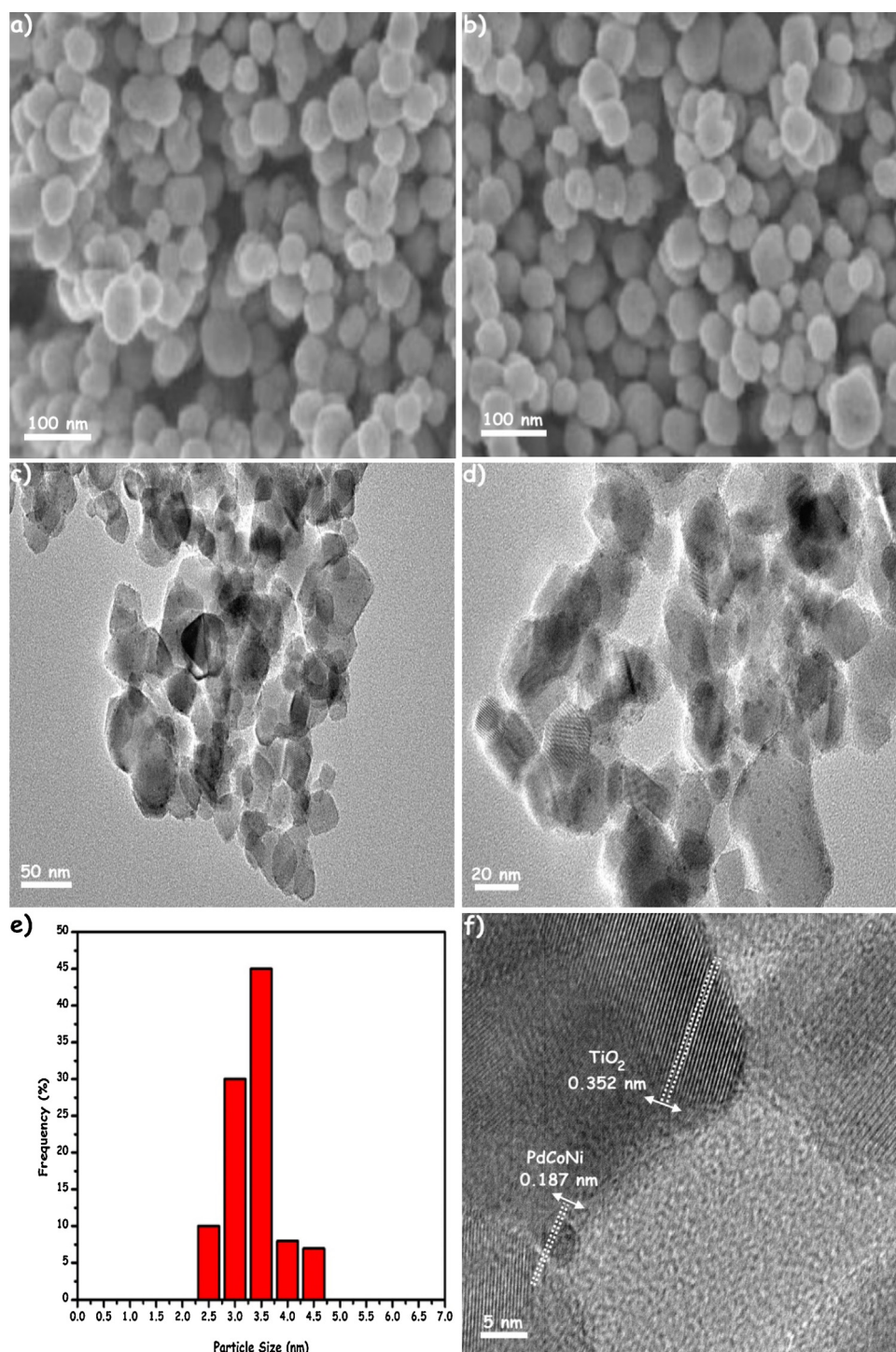
Fig. 2. a)-b) FESEM images of $Pd_{0.60}Co_{0.18}Ni_{0.22}/TiO_2$ taken from different regions, c)-d) BFTEM images of $Pd_{0.60}Co_{0.18}Ni_{0.22}/TiO_2$ in different magnifications, e) corresponding size histogram of $Pd_{0.60}Co_{0.18}Ni_{0.22}/TiO_2$ and f) HRTEM image of $Pd_{0.60}Co_{0.18}Ni_{0.22}/TiO_2$ sample.

ascribed to its special composition and surface electronic state in the formed alloy structure [51–53], which was further supported by the result of a control experiment in which the physical mixture of $Pd_{0.60}/TiO_2$, $Co_{0.21}/TiO_2$ and $Ni_{0.22}/TiO_2$ exhibits lower activity than the $Pd_{0.60}Co_{0.18}Ni_{0.22}/TiO_2$ catalyst in FA dehydrogenation under identical conditions (**Fig. S4**, Supporting Information). The gas generated from $Pd_{0.60}Co_{0.18}Ni_{0.22}/TiO_2$ catalyzed FA dehydrogenation was analyzed by gas chromatography (GC), infrared spectroscopy (FTIR) and NaOH trap experiment (**Fig. S5**, Supporting Information). Their results evidenced that the generated gas is a mixture of H_2

and CO_2 with a H_2:CO_2 molar ratio of 1.0:1.0 where CO was below the detection limit (*i.e.* <10 ppm).

In another control experiment, we checked the catalytic reactivity of $Pd_{0.60}Co_{0.18}Ni_{0.22}/TiO_2$ in the hydrolytic dehydrogenation of sodium formate (SF) for why in our catalytic system we used SF as a promoter to enhance the rate of formic acid decomposition as reported in many previous studies [20,26,38]. In this context, the recent reports have pointed out that some homogeneous [59] and heterogeneous [60] catalysts can liberate H_2 not only from FA but also SF through a catalytic hydrolysis of SF (4).
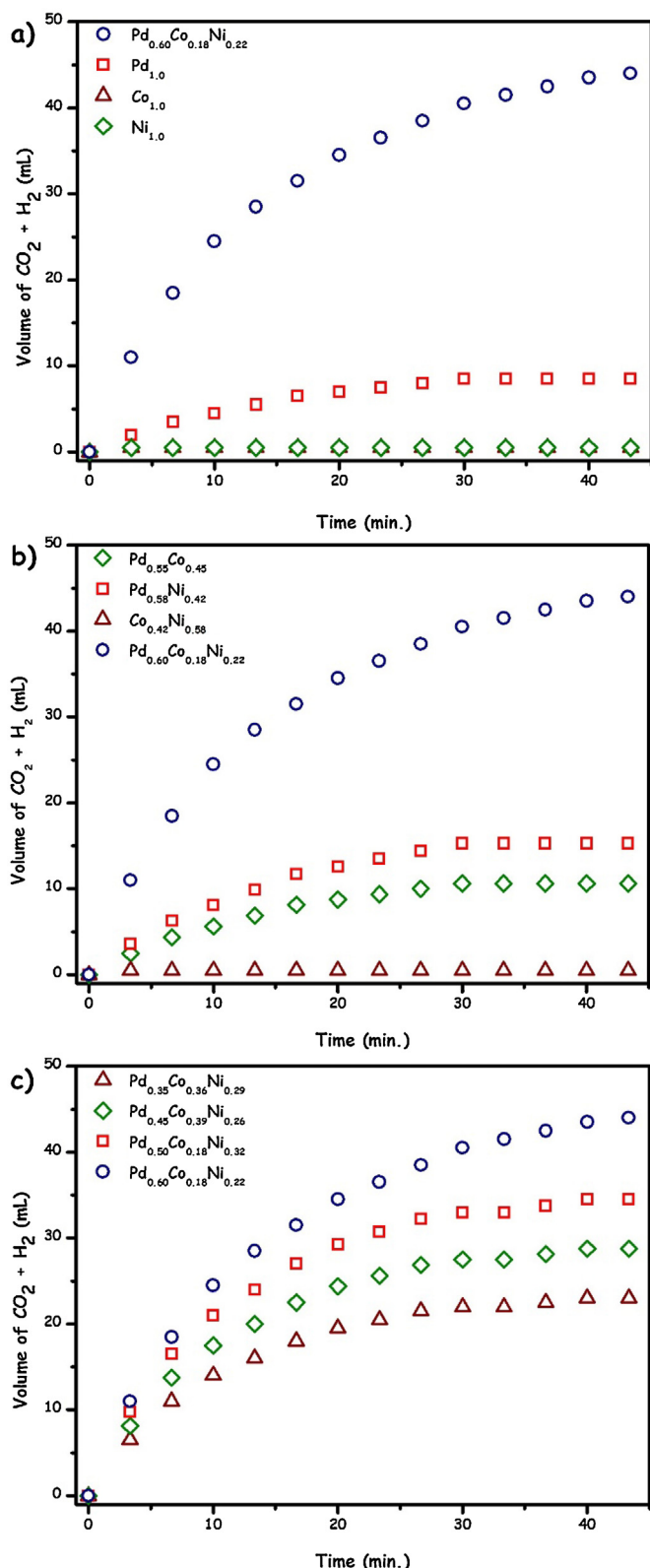
Fig. 3. Volume of generated gas ($CO_2 + H_2$) (mL) versus time (min) graphs obtained by a) monometallic, b) bimetallic, c) trimetallic catalysts in different [Pd]:[Co]:[Ni] ratios for the FA dehydrogenation (0.175 M FA + 0.175 M SF) at room temperature.

For this reason we checked whether $Pd_{0.60}Co_{0.18}Ni_{0.22}/TiO_2$ catalyze the hydrolysis of SF. The result of this experiment showed that $Pd_{0.60}Co_{0.18}Ni_{0.22}/TiO_2$ catalyzed hydrolysis of SF only produces 2.5 mL hydrogen gas over 4 h at room temperature, which was correlated for all data collected in $Pd_{0.60}Co_{0.18}Ni_{0.22}/TiO_2$ catalyzed dehydrogenation of FA.

$$HCOONa + H_2O \rightarrow H_2 + NaHCO_3 \qquad (4)$$
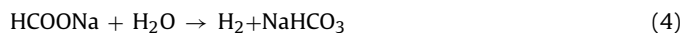
In order to shed some light on the effect of alloying on the catalytic reactivity of PdCoNi alloy NPs in FA dehydrogenation, linear sweep voltammetry (LSV) and CO stripping voltammetry analyses were performed over $Pd_{0.60}Co_{0.18}Ni_{0.22}/TiO_2$, $Pd_{0.60}/TiO_2$, $Pd_{0.58}Ni_{0.42}/TiO_2$ and $Pd_{0.55}Co_{0.45}/TiO_2$ nanocatalysts. Firstly, LSV measurements on $Pd_{0.60}/TiO_2$, $Pd_{0.58}Ni_{0.42}/TiO_2$, $Pd_{0.55}Co_{0.45}/TiO_2$ and $Pd_{0.60}Co_{0.18}Ni_{0.22}/TiO_2$ nanocatalysts were conducted to understand their stability in the FA electrooxidation. For this purpose, the catalysts were electrochemically pretreated before the LSV measurements by using a bias potential of 0.0 V for 0–500 s, where CO and OH intermediates form and bind to the active surface sites of catalysts [61]. Afterward, LSV measurements were implemented on the poisoned catalysts surfaces, in which the maximum current versus potential values were recorded as a function of the poisoning time (Fig. 4(a–d)). It is seen that $Pd_{0.60}Co_{0.18}Ni_{0.22}/TiO_2$ nanocatalyst has characteristically higher activity than $Pd_{0.60}/TiO_2$, $Pd_{0.58}Ni_{0.42}/TiO_2$ and $Pd_{0.55}Co_{0.45}/TiO_2$ nanocatalysts toward formic acid oxidation in terms of peak current values. Moreover, examination of the relative peak current versus poisoning time (Fig. 4 (e)) suggests that while $Pd_{0.60}/TiO_2$ nanocatalyst loses its >30% of its activity upon 500 s of poisoning; $Pd_{0.60}Co_{0.18}Ni_{0.22}/TiO_2$ nanocatalyst retains >92% of its initial activity after an identical poisoning treatment. Fig. 5 gives CO-stripping voltammograms for $Pd_{0.60}/TiO_2$, $Pd_{0.58}Ni_{0.42}/TiO_2$, $Pd_{0.55}Co_{0.45}/TiO_2$ and $Pd_{0.60}Co_{0.18}Ni_{0.22}/TiO_2$ nanocatalysts. The onset potentials were found to be 0.68, 0.51, 0.50 and 0.48 V for $Pd_{0.60}/TiO_2$, $Pd_{0.55}Co_{0.45}/TiO_2$, $Pd_{0.58}Ni_{0.42}/TiO_2$ and $Pd_{0.60}Co_{0.18}Ni_{0.22}/TiO_2$, respectively. In the light of the previous reports [62,63], where even smaller energy differences ($\Delta V_{COads} \leq 70$ mV) were reported, this result clearly demonstrates that the CO poisoning resistivity of PdCoNi alloy NPs higher than Pd based bimetallic ($PdCo/TiO_2$, $PdNi/TiO_2$) and monometallic (Pd/TiO_2) NPs.

3.3. ALD-SiO₂ layer protection of TiO₂ supported PdCoNi NPs and their catalytic performance in formic acid dehydrogenation

With the optimum catalyst composition in the hand, we utilized ALD technique for growing SiO_2 layers between PdCoNi alloy NPs to protect them against to sintering and leaching in the dehydrogenation of FA. An outline of the our followed synthetic strategy [64,65] is depicted in Scheme 1, which involves (1) the preparation of PdCoNi alloy NPs via wet-impregnation-reduction method, (2) their surface protection with oleylamine (OAm) blocking agent, (3) the growing of SiO_2 layers up to optimum thickness for catalysis by ALD and (4) removing of oleylamine (OAm) blocking agent through acetic acid washing followed by calcination. SiO_2 layers between PdCoNi alloys NPs supported on TiO_2 nanopowders were generated using sequential exposures to 3-aminopropyltriethoxysilane (APTS) and water (H_2O) vapors. Different numbers of SiO_2-ALD cycles (1–20) were performed to generate protective layers of progressively increasing thickness on $Pd_{0.60}Co_{0.18}Ni_{0.22}/TiO_2$ nanocatalyst. A simplified description of the sequential deposition of aminosilane and water vapor on TiO_2 surface is also shown in Scheme 2.

The catalytic activities of the resulting materials taken at the end of 1, 2, 4, 6, 10 and 20 cycles of SiO_2-ALD processes were examined in the dehydrogenation of aqueous FA solution
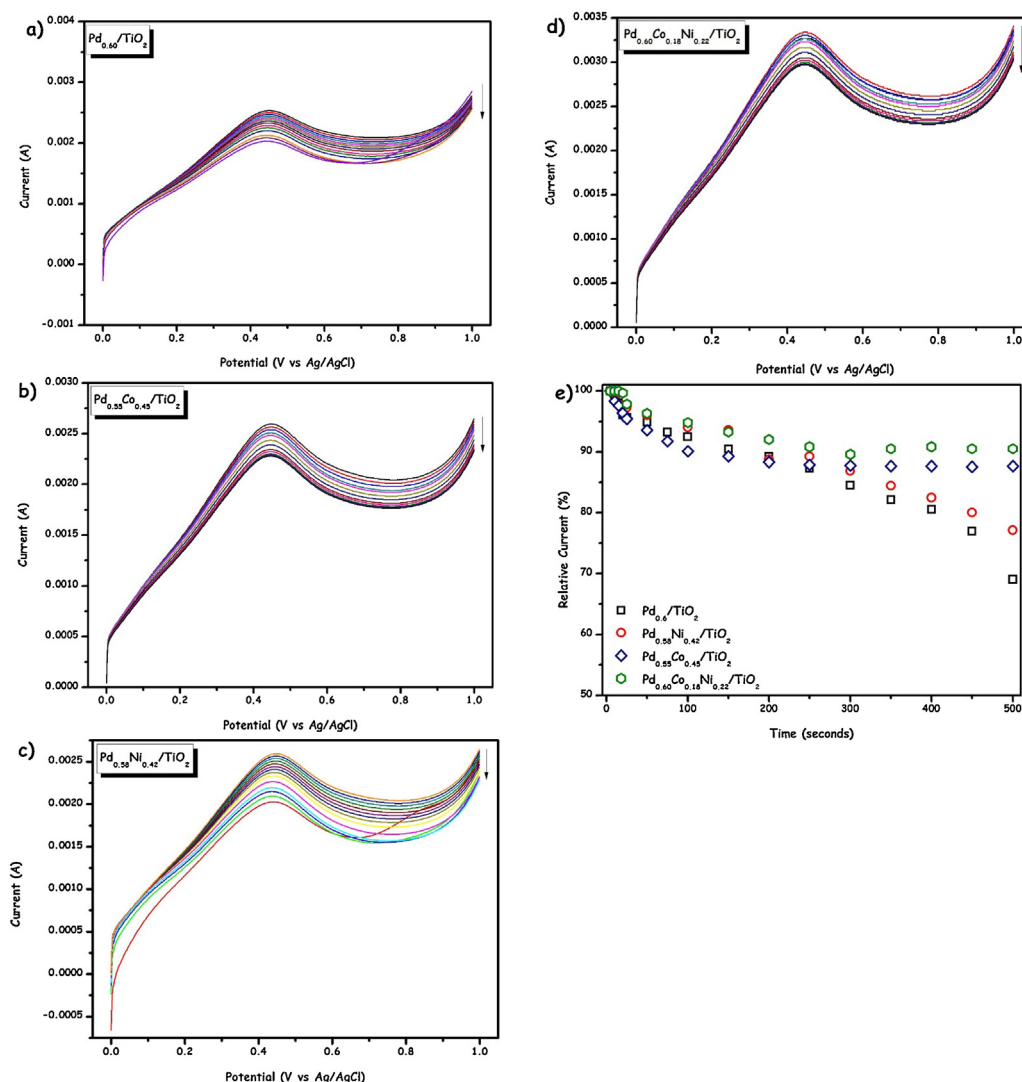
Fig. 4. LSV measurements on a) $Pd_{0.60}/TiO_2$, b) $Pd_{0.55}Co_{0.45}/TiO_2$, c) $Pd_{0.58}Ni_{0.42}/TiO_2$, d) $Pd_{0.60}Co_{0.18}Ni_{0.22}/TiO_2$ nanocatalysts in 0.5 M H_2SO_4 + 1 M HCOOH solution with a 10 mVs^{-1} scan rate, e) the relative maximum peak current vs time graph for $Pd_{0.60}/TiO_2$, $Pd_{0.55}Co_{0.45}/TiO_2$, $Pd_{0.58}Ni_{0.42}/TiO_2$, $Pd_{0.60}Co_{0.18}Ni_{0.22}/TiO_2$ nanocatalysts.

(0.175 M FA + 0.175 M SF) at room temperature. The observed gas generation rates with respect to SiO_2-ALD cycles are given in Fig. 6(a). The observed enhancement in the catalytic activities of $Pd_{0.60}Co_{0.18}Ni_{0.22}/TiO_2$-ALD-$SiO_2$ samples up to 10 ALD-SiO_2 cycles can be explained by the existence of free amine groups (from APTS) in the catalytic material, whereas the lowest activity obtained by $Pd_{0.60}Co_{0.18}Ni_{0.22}/TiO_2$-ALD-$SiO_2$ (20 cycles) can be ascribed to over coating of PdCoNi alloy NPs with SiO_2 (*vide infra*). The existence of −NH_2 functionalities grafted onto support enhances the activity of active Pd nanoparticles by affecting the FA adsorption/storage process. In their pioneering study, Yamashita et al. [66] reported that a resin bearing −$N(CH_3)_2$ acted as a significantly more efficient organic support material in the catalytic decomposition of FA than those bearing −SO_3H, −COOH, and −OH. Their mechanistic studies revealed that O−H bond cleavage in FA is facilitated by the −$N(CH_3)_2$ functionalities leading to the formation of metal-bound formate species along with a −$[N(CH_3)_2H]^+$ species, followed by the dehydrogenation of the metal-bound formate, producing H_2 and CO_2. More recently, this strong interaction between metal nanoparticles and amine group grafted on support material has been named as "Strong Metal-Molecular Support Interaction" (SMMSI) by Yadav et al. [67].

Amongst $Pd_{0.60}Co_{0.18}Ni_{0.22}/TiO_2$-ALD-$SiO_2$ (1, 2, 4, 6, 10 and 20 cycles) materials the highest catalytic performance in terms of both activity and conversion was achieved by $Pd_{0.60}Co_{0.18}Ni_{0.22}/TiO_2$-ALD-$SiO_2$ (6 cycles); this nanocatalyst catalyzes the room temperature dehydrogenation of aqueous FA solution (0.175 M FA + 0.175 M SF) with an *initial* turnover frequency (TOF) value of 207 mol H_2/mol (Pd + Co + Ni) × h at >99% selectivity and nearly complete conversion. This activity value is almost 2 times higher than that of obtained by $Pd_{0.60}Co_{0.18}Ni_{0.22}/TiO_2$ (110 mol H_2/mol (Pd + Co + Ni) × h) at 60% conversion (Fig. 6(b)). Moreover, the inspection of the literature shows that $Pd_{0.60}Co_{0.18}Ni_{0.22}/TiO_2$-ALD-$SiO_2$ (6 cycles) nanocatalyst provides higher TOF value (207 mol H_2/mol (Pd + Co + Ni) × h; uncorrected for surface exposed active PdCoNi sites) than the previously reported PdNiAg/C (85 mol H_2/mol catalyst × h at 50 °C) [38], Au-Pd/ED-MIL-101 (49 mol H_2/mol catalyst × h at 90 °C) [68], Pd@SiO_2 (70 mol H_2/mol catalyst × h at 90 °C) [69], Au/Al_2O_3 (64 mol H_2/mol catalyst × h at 50 °C) [70], Pd-Au/C (27 mol H_2/mol catalyst × h at 92 °C) [71], PdAu@Au/C (45 mol H_2/mol catalyst × h at 92 °C) [71] and PdNi@Pd/GNs-CB (66 mol H_2/mol catalyst × h at 25 °C) [72] NPs tested in the dehydrogenation of FA by using SF as a promoter.

The compositional, structural and morphological characterization of the resulting $Pd_{0.60}Co_{0.18}Ni_{0.22}/TiO_2$-ALD-$SiO_2$ (6 cycles)
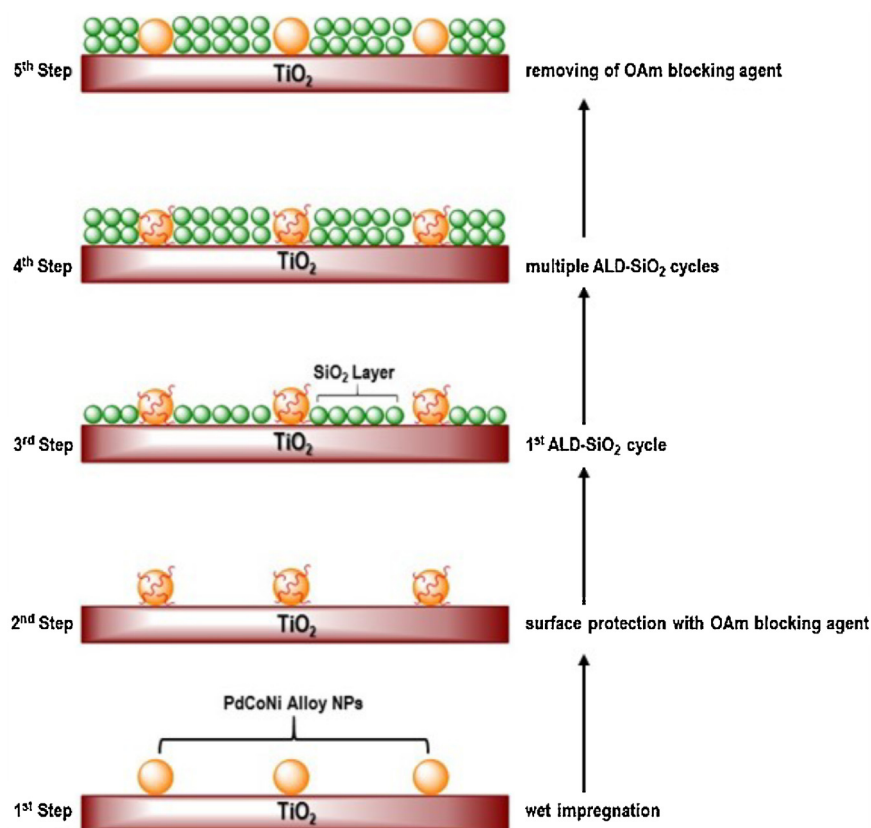
Scheme 1. The synthesis protocol followed in the preparation of ALD-SiO$_2$ layers protected PdCoNi alloy NPs supported on TiO$_2$ nanopowders.
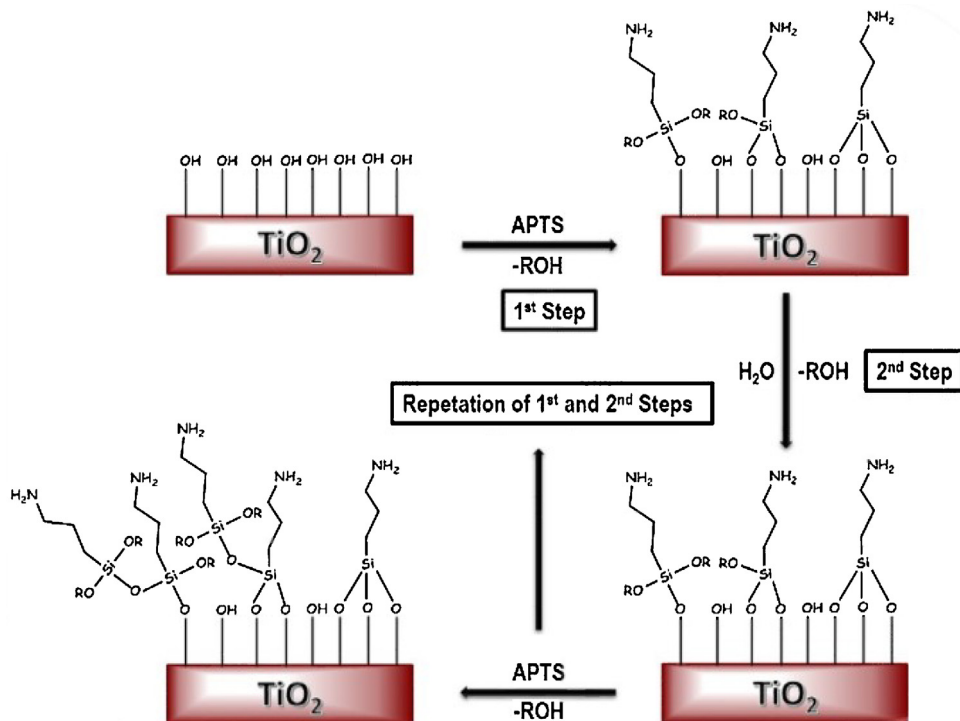
Scheme 2. A schematically description of the ALD-sequential deposition of aminosilane and water vapor on the TiO$_2$ surface.

was done by P-XRD, ATR-IR, BFTEM, HRTEM and HAADF-STEM-point analyses. ICP-OES analysis of Pd$_{0.60}$Co$_{0.18}$Ni$_{0.22}$/TiO$_2$-ALD-SiO$_2$ revealed that the retaining of the same metal composition upon ALD-SiO$_2$ process (1.78% wt Pd, 0.29% wt Co, and 0.36% wt Ni

loadings correspond to 24.0 μmol Pd, 7.2 μmol Co and 8.8 μmol Ni) in Pd$_{0.60}$Co$_{0.18}$Ni$_{0.22}$/TiO$_2$-ALD-SiO$_2$ (6 cycles) sample. P-XRD pattern of Pd$_{0.60}$Co$_{0.18}$Ni$_{0.22}$/TiO$_2$-ALD-SiO$_2$ (6 cycles) was found to be identical with that of Pd$_{0.60}$Co$_{0.18}$Ni$_{0.22}$/TiO$_2$ (**Fig. S6**, Supporting

Fig. 6. a) The rate of gas generation (($CO_2 + H_2$) mL/min) versus time no of ALD-SiO$_2$ cycles obtained by Pd$_{0.60}$Co$_{0.18}$Ni$_{0.22}$/TiO$_2$-ALD-SiO$_2$ (1–20 cycles) nanocatalysts for the FA dehydrogenation (0.175 M FA + 0.175 M SF) at room temperature, b) the volume generated gas ($CO_2 + H_2$) (mL) versus time (min) graphs for Pd$_{0.60}$Co$_{0.18}$Ni$_{0.22}$/TiO$_2$-ALD-SiO$_2$ (6 cycles) and Pd$_{0.60}$Co$_{0.18}$Ni$_{0.22}$/TiO$_2$ nanocatalysts catalyzed FA dehydrogenation (0.175 M FA + 0.175 M SF) at room temperature.

Fig. 5. CO stripping voltammograms of a) Pd$_{0.60}$/TiO$_2$, b) Pd$_{0.55}$Co$_{0.45}$/TiO$_2$, c) Pd$_{0.58}$Ni$_{0.42}$/TiO$_2$, d) Pd$_{0.60}$Co$_{0.18}$Ni$_{0.22}$/TiO$_2$ nanocatalysts in H$_2$SO$_4$ solution with a 10 mVs^{-1} scan rate.

Information) indicative of the crystallinity of the host material (TiO$_2$ nanopowders) remains intact at the end of the ALD-SiO$_2$ process. The comparison of ATR-IR spectra of Pd$_{0.60}$Co$_{0.18}$Ni$_{0.22}$/TiO$_2$-ALD-SiO$_2$ (6 cycles) and Pd$_{0.60}$Co$_{0.18}$Ni$_{0.22}$/TiO$_2$ samples pointed to the existence of APTS on the resultant Pd$_{0.60}$Co$_{0.18}$Ni$_{0.22}$/TiO$_2$-ALD-SiO$_2$ sample (**Fig. S7**, Supporting Information) with its characteristics −NH$_2$ bending and N−H stretching vibrations around 1500 and 3300 cm^{-1}, respectively [73].

BFTEM images of Pd$_{0.60}$Co$_{0.18}$Ni$_{0.22}$/TiO$_2$-ALD-SiO$_2$ (6 cycles) are given in Fig. 7(a) and (b). As seen from these images the shape of the resulting PdCoNi NPs was not changed by ALD-SiO$_2$ process and only their mean size increased from 3.45 nm to 3.52 nm (Fig. 7(c)). HAADF-STEM-EDX point analyses of Pd$_{0.60}$Co$_{0.18}$Ni$_{0.22}$/TiO$_2$-ALD-SiO$_2$ (6 cycles) nanocatalyst were performed on two separated NPs and their results are given in Fig. 7(d). STEM-EDX spectrum collected from these two NPs exhibited that the presence of Pd, Co and Ni metals in the analyzed NPs, which reveals that the preservation of PdCoNi alloy structure in Pd$_{0.60}$Co$_{0.18}$Ni$_{0.22}$/TiO$_2$-ALD-SiO$_2$ (6 cycles) sample. Fig. 8 shows HRTEM images of Pd$_{0.60}$Co$_{0.18}$Ni$_{0.22}$/TiO$_2$-ALD-SiO$_2$ (6, 10, 20 cycles) nanocatalysts. The existence of SiO$_2$ layer is easily seen from HRTEM image of Pd$_{0.60}$Co$_{0.18}$Ni$_{0.22}$/TiO$_2$-ALD-SiO$_2$ (10 cycles) sample and the crystalline fringe distance of SiO$_2$ layers protected PdCoNi NPs was measured to be 0.189, which differs from [111] spacing of the face-
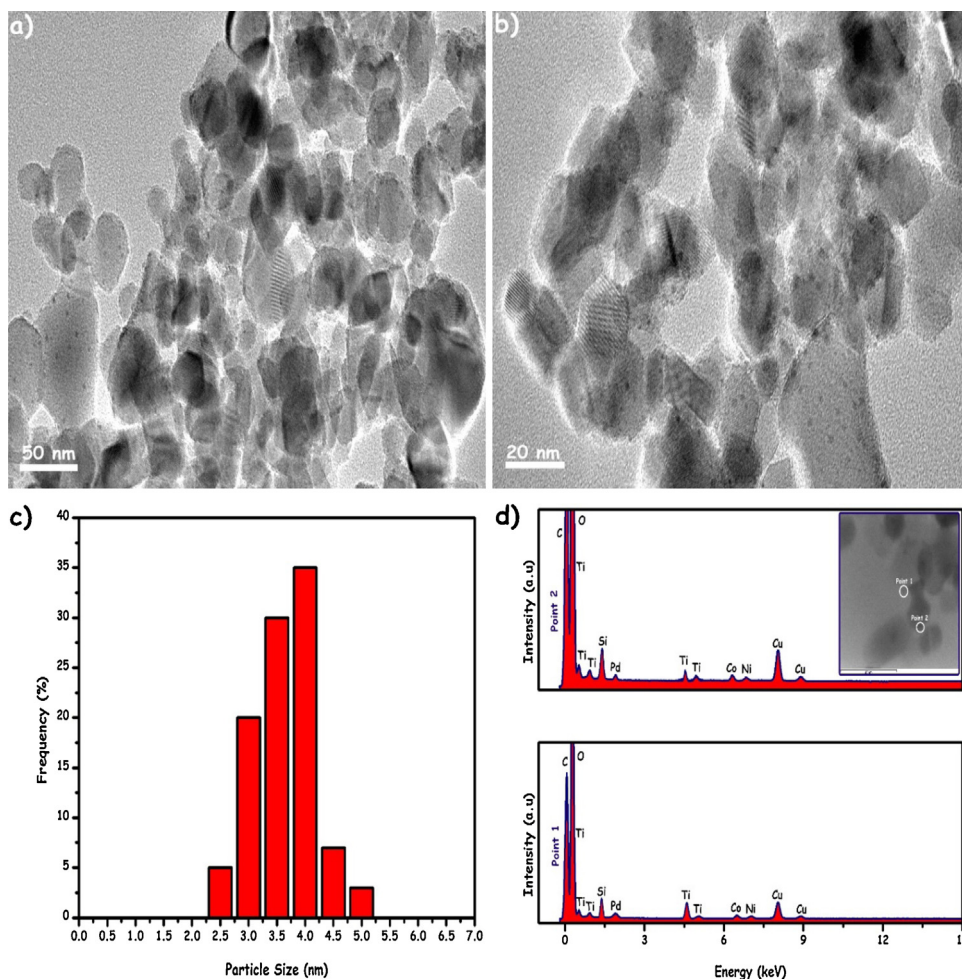
Fig. 7. a), b) BFTEM images of $Pd_{0.60}Co_{0.18}Ni_{0.22}/TiO_2$-ALD-SiO$_2$ (6 cycles) nanocatalyst, c) the corresponding size histogram of $Pd_{0.60}Co_{0.18}Ni_{0.22}/TiO_2$-ALD-SiO$_2$ (6 cycles) nanocatalyst, d) HAADF-STEM image (inset) and STEM-EDX spectra of $Pd_{0.60}Co_{0.18}Ni_{0.22}/TiO_2$-ALD-SiO$_2$ (6 cycles) nanocatalyst collected from two separate particles indicated in HAADF-STEM image.

centered cubic (*fcc*) Pd (0.22 nm) [33], Ni (0.28 nm) [38] and Co (0.21 nm) [58] and can readily be assigned to PdCoNi alloy structure [56]. The lowest activity of $Pd_{0.60}Co_{0.18}Ni_{0.22}/TiO_2$-ALD-SiO$_2$ (20 cycles) in FA dehydrogenation can be explained by considering its HRTEM image given in Fig. 8(c) as it shows that the existence of highly clumped PdCoNi NPs and their over-coating with SiO$_2$ layers through ALD-SiO$_2$ process, which blocks the active sites of PdCoNi NPs.

The isolability and reusability performances of $Pd_{0.60}Co_{0.18}Ni_{0.22}/TiO_2$ and $Pd_{0.60}Co_{0.18}Ni_{0.22}/TiO_2$-ALD-SiO$_2$ (6 cycles) nanocatalysts, as two critical measures in heterogeneous catalysis, were tested in the dehydrogenation of aqueous FA solution (0.175 M FA + 0.175 M SF) at 100 °C. The main reason of working on high temperature instead of doing this test at room temperature was to see the durability of PdCoNi NPs against to sintering and leaching in $Pd_{0.60}Co_{0.18}Ni_{0.22}/TiO_2$ and $Pd_{0.60}Co_{0.18}Ni_{0.22}/TiO_2$-ALD-SiO$_2$ (6 cycles) nanocatalysts, respectively. After completion of 1st run in FA dehydrogenation, $Pd_{0.60}Co_{0.18}Ni_{0.22}/TiO_2$ and $Pd_{0.60}Co_{0.18}Ni_{0.22}/TiO_2$-ALD-SiO$_2$ (6 cycles) were isolated as black powder by suction filtration, washed with ethanol/water, and dried vacuum-oven under 10^{-1} Torr at 50 °C. The solid samples of $Pd_{0.60}Co_{0.18}Ni_{0.22}/TiO_2$ and $Pd_{0.60}Co_{0.18}Ni_{0.22}/TiO_2$-ALD-SiO$_2$ (6 cycles) can be bottled and stored under inert atmosphere. Furthermore, when reused $Pd_{0.60}Co_{0.18}Ni_{0.22}/TiO_2$-ALD-SiO$_2$ (6 cycles) is still acting as highly active and selective nanocatalyst in the dehydrogenation of FA by retaining ≥83% of the initial catalytic

without jeopardizing the selectivity even at the 20th catalytic reuse, whereas $Pd_{0.60}Co_{0.18}Ni_{0.22}/TiO_2$ completely lost its catalytic performance (activity, selectivity and conversion) (Fig. 9(a)). This result can also be translated into lower bound total turnover number (TTON) of 643 mol H$_2$/mol metal.

The morphological investigation of the recovered catalysts $Pd_{0.60}Co_{0.18}Ni_{0.22}/TiO_2$-ALD-SiO$_2$ (6 cycles) and $Pd_{0.60}Co_{0.18}Ni_{0.22}/TiO_2$ from 20th reuse was performed by taking their BFTEM images (Fig. 9(b) and (c)). As seen from these images $Pd_{0.60}Co_{0.18}Ni_{0.22}/TiO_2$-ALD-SiO$_2$ (6 cycles) provided great stability against to sintering throughout the reusability experiments, their mean size just increased from 3.52 to 3.75 nm that explains the slight decrease in the catalytic performance at 20th reuse, while PdCoNi alloy NPs in $Pd_{0.60}Co_{0.18}Ni_{0.22}/TiO_2$ were found to be highly agglomerated as a result of their sintering on the surface of TiO$_2$.

The leaching possibility of PdCoNi alloy NPs in $Pd_{0.60}Co_{0.18}Ni_{0.22}/TiO_2$-ALD-SiO$_2$ (6 cycles) nanocatalyst was also examined by performing ICP-OES analyses on aliquots of reaction solutions taken at the end of 5th, 10th and 20th reuse, that no Pd, Co and Ni was detected in these solutions confirms that the retention of metals on the surface of TiO$_2$. Taking all the results together one can conclude that $Pd_{0.60}Co_{0.18}Ni_{0.22}/TiO_2$-ALD-SiO$_2$ (6 cycles) nanocatalyst resulting from 6 cycles ALD-SiO$_2$ coating of $Pd_{0.60}Co_{0.18}Ni_{0.22}/TiO_2$ is isolable, bottleable, redispersible, and repeatedly usable as an active nanocatalyst for the dehydrogenation of aqueous FA solution and growing of SiO$_2$ layers among
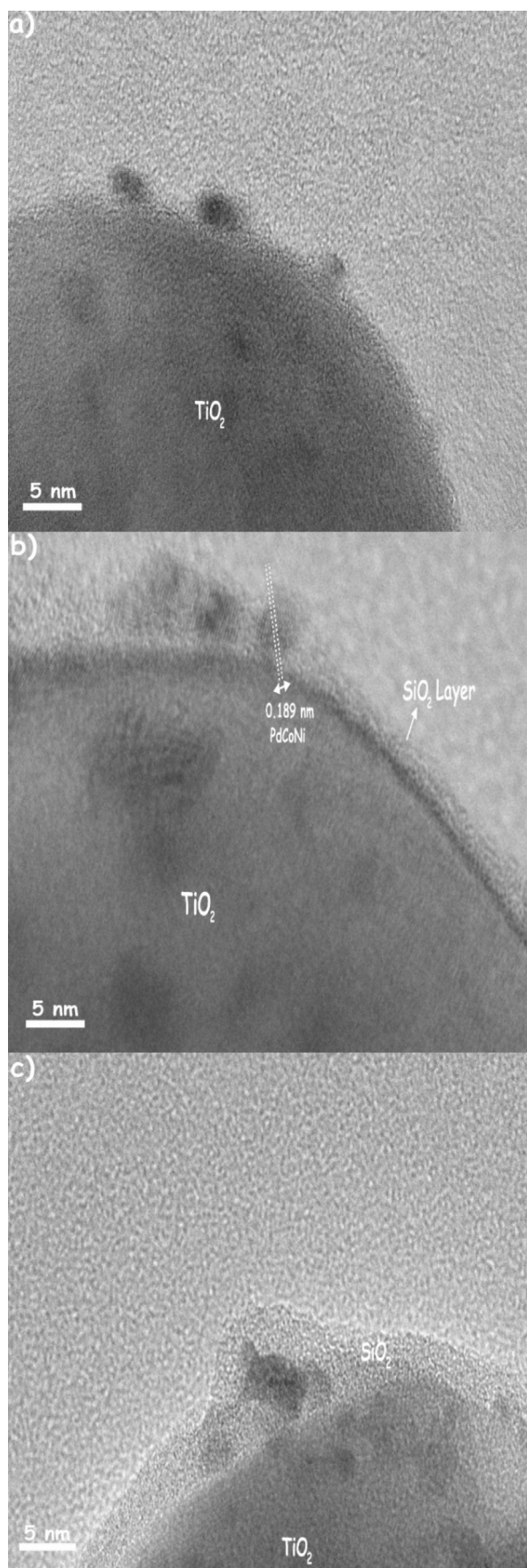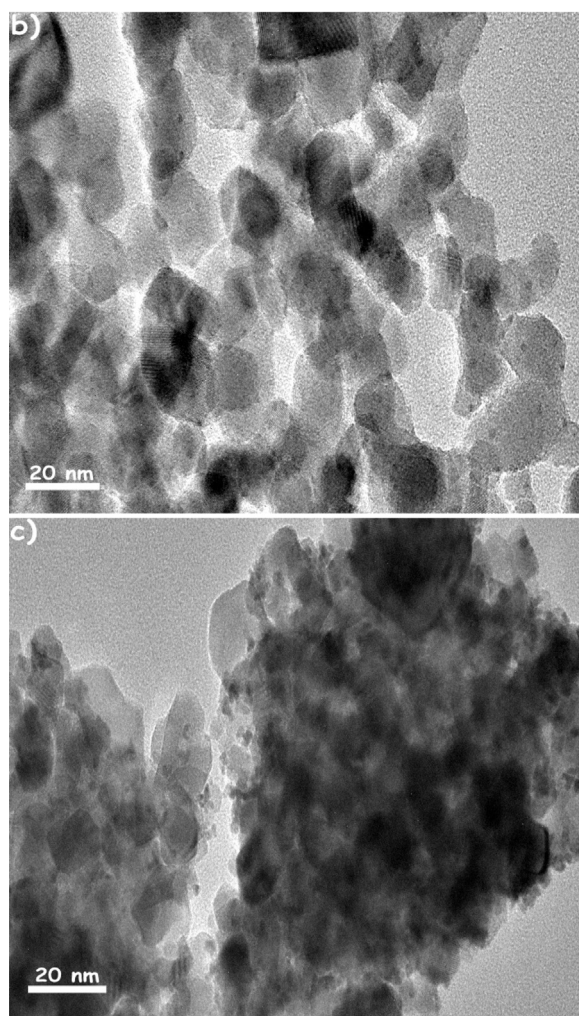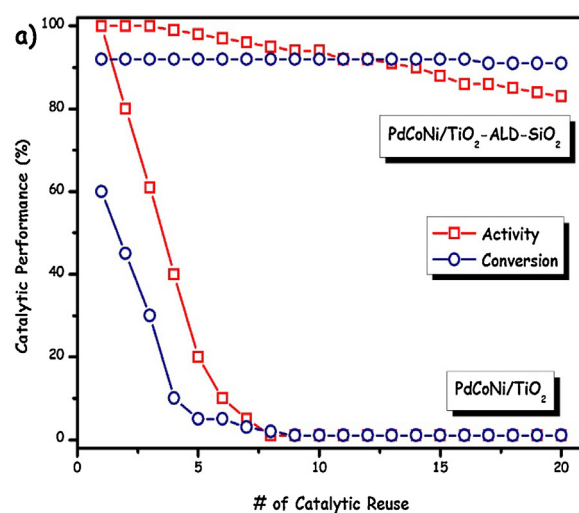
Fig. 9. a) The percentage of retained catalytic performance versus no of catalytic reuse for $Pd_{0.60}Co_{0.18}Ni_{0.22}/TiO_2$ and $Pd_{0.60}Co_{0.18}Ni_{0.22}/TiO_2$-ALD-SiO$_2$ (6 cycles) catalyzed FA dehydrogenation (0.175 M FA + 0.175 M SF) at room temperature, b) and c) BFTEM images of HRTEM images of $Pd_{0.60}Co_{0.18}Ni_{0.22}/TiO_2$-ALD-SiO$_2$ (6 cycles) and $Pd_{0.60}Co_{0.18}Ni_{0.22}/TiO_2$ nanocatalysts, respectively recovered at the end of 20th catalytic reuse.

Fig. 8. HRTEM images of a) $Pd_{0.60}Co_{0.18}Ni_{0.22}/TiO_2$-ALD-SiO$_2$ (6 cycles), b) $Pd_{0.60}Co_{0.18}Ni_{0.22}/TiO_2$-ALD-SiO$_2$ (10 cycles), c) $Pd_{0.60}Co_{0.18}Ni_{0.22}/TiO_2$-ALD-SiO$_2$ (20 cycles) nanocatalysts.

PdCoNi alloy NPs momentously enhances the stability of TiO$_2$ surface bound PdCoNi alloy NPs against to sintering and leaching. It should also be noted that the reusability performance of Pd$_{0.60}$Co$_{0.18}$Ni$_{0.22}$/TiO$_2$-ALD-SiO$_2$ (6 cycles) can also be translated into a lower bound total turnover number (TTON) of $\geq$7500 mol H$_2$/mol catalyst and to the best of our knowledge this is the highest TTON value reported up to date for the FA dehydrogenation at room temperature.

4. Conclusions

In the current study, ALD-SiO$_2$ layers protected PdCoNi alloy NPs supported on TiO$_2$ nanopowders were prepared, characterized and used as nanocatalyst in the dehydrogenation of FA by using SF as a promoter. Some of the major findings of this study can be summarized as follows:

(a) For the first time, trimetallic PdCoNi NPs supported on TiO$_2$ nanopowders (PdCoNi/TiO$_2$) were prepared by wet-impregnation followed by simultaneous reduction method. PdCoNi/TiO$_2$ nanocatalyst was characterized by using ICP-OES, P-XRD, HR-XPS, FE-SEM, BFTEM, HRTEM, HAADF-STEM and STEM-EDX analyses. The results of these multi-pronged analyses elicit that the formation of well-dispersed and highly crystalline PdCoNi NPs in alloy structure on the surface of TiO$_2$ matrix,

(b) The catalytic employment of PdCoNi/TiO$_2$ was demonstrated in the FA dehydrogenation by using SF as a promoter. We found that trimetallic PdCoNi alloy NPs provide better activity than that of obtained by monometallic (Pd/TiO$_2$, Co/TiO$_2$, Ni/TiO$_2$) and bimetallic (PdCo/TiO$_2$, PdNi/TiO$_2$, CoNi/TiO$_2$) counterparts. LSV and CO-stripping voltammetry analyses evidenced that trimetallic PdCoNi alloy NPs has higher resistivity against to poisonous CO and OH intermediates than their mono-and bimetallic compositions, which explains the enhanced activity of PdCoNi/TiO$_2$ in FA dehydrogenation,

(c) ALD was utilized to improve the catalytic durability of PdCoNi/TiO$_2$ by growing SiO$_2$ layers among PdCoNi alloy NPs by using APTS and OAm as silica source and surface protecting group, respectively. Thanks to the existence of free —NH$_2$ functionalities (from APTS) the resulting Pd$_{0.60}$Co$_{0.18}$Ni$_{0.22}$/TiO$_2$-ALD-SiO$_2$ (6 cycles) nanocatalyst displays almost two times higher activity than Pd$_{0.60}$Co$_{0.18}$Ni$_{0.22}$/TiO$_2$ in FA dehydrogenation at room temperature by providing an initial turnover frequency (TOF) value of 207 mol H$_2$/mol (Pd + Co + Ni) × h at >99% dehydrogenation selectivity and almost complete conversion,

(d) Moreover, these SiO$_2$ layer protected PdCoNi alloy NPs showed previously unprecedented catalytic stability against to sintering and leaching throughout the reusability experiments so that they retain $\geq$83% of their catalytic activity and selectivity at >90% catalytic conversion even at the 20th catalytic reuse under forcing conditions, whereas Pd$_{0.60}$Co$_{0.18}$Ni$_{0.22}$/TiO$_2$ completely lost its catalytic reactivity.

In summary, this new highly stable and efficient catalytic system can strongly promote the practical applications of formic acid as a CO-free H$_2$ generation system for fuel cell applications.

Acknowledgement

Appendix A. Supplementary data

Supplementary data associated with this article can be found, in the online version, at http://dx.doi.org/10.1016/j.apcatb.2017.04.022.

References

[1] Principles and Practice of Heterogeneous Catalysis, in: J.M. Thomas, W.J. Thomas (Eds.), VCH Publishing, Weinheim, Germany, 1997.
[2] M. Zahmakiran, S. Ozkar, Nanoscale 3 (2011) 3462.
[3] Sustainale Preparation of Metal Nanoparticles: Methods and Applications, in: R. Luque, R.S. Varma (Eds.), RSC Publishing, London UK, 2012.
[4] R.J. White, R. Luque, V.L. Budarin, J.H. Clark, D.J. Macquarrie, Chem. Soc. Rev. 38 (2009) 481.
[5] J.M. Campelo, D. Luna, R. Luque, J.M. Marinas, A.A. Romero, ChemSusChem 2 (2009) 18.
[6] D. Astruc, F. Lu, J.R. Aranzaes, Angew. Chem. Int. Ed. 44 (2005) 7852.
[7] J.-N. Park, A.J. Forman, W. Tang, J. Cheng, Y.-S. Hu, H. Lin, E.W. McFarland, Small 4 (2008) 1694.
[8] T. Kanazawa, Catal. Lett. 108 (2006) 45.
[9] S. Takenaka, H. Matsumori, K. Nakagawa, H. Matsune, E. Tanabe, M. Kishida, J. Phys. Chem. A 111 (2007) 15133.
[10] M. Zhao, L. Sun, R.M. Crooks, J. Am. Chem. Soc. 120 (1998) 4877.
[11] P.M. Arnal, M. Comotti, F. Schuth, Angew. Chem. Int. Ed. 45 (2006) 8224.
[12] S.H. Joo, J.Y. Park, C.-K. Tsung, Y. Yamada, P. Yang, G.A. Somorjai, Nat. Mater. 8 (2009) 126.
[13] S.M. George, Chem. Rev. 110 (2010) 111.
[14] H. Feng, J.W. Elam, J.A. Libera, W. Setthapun, P.C. Stair, Chem. Mater. 22 (2010) 3133.
[15] H. Feng, J. Lu, P.C. Stair, J.W. Elam, Catal. Lett. 141 (2011) 512.
[16] N.A. Ray, R.P.V. Duyne, P.C. Stair, J. Phys. Chem. C 116 (2012) 7748.
[17] T. Schaub, R.A. Paciello, Angew. Chem. Int. Ed. 50 (2011) 7278.
[18] D. Preti, C. Resta, S. Squarcialupi, G. Faschinetti, Angew. Chem. Int. Ed. 50 (2011) 12551.
[19] S. Enthaler, J.V. Langermann, T. Schmidt, Energy Environ. Sci. 3 (2010) 1207–1217.
[20] M. Yadav, Q. Xu, Energy Environ. Sci. 5 (2012) 9698–9725.
[21] K.V. Kordesch, G.R. Simader, G. R. Chem. Rev. 95 (1995) 191.
[22] T.C. Johnson, D.J. Morris, M. Wills, Chem. Soc. Rev. 39 (2010) 81.
[23] M. Grasemann, G. Laurenzcy, Energy Environ. Sci. 5 (2012) 8171.
[24] S. Fukuzimi, T. Kobayashi, T. Suenobu, J. Am. Chem. Soc. 132 (2010) 1496.
[25] A. Boddien, D. Mellmann, F. Gaertner, R. Jackstell, H. Junge, P.J. Dyson, G. Laurenczy, R. Ludwig, M. Beller, Science 333 (2011) 1733.
[26] Q.L. Zhu, N. Tsumori, Q. Xu, Chem. Sci. 5 (2014) 195.
[27] X. Zhou, Y. Huang, W. Xing, C. Liu, J. Liao, T. Lu, Chem. Commun. (2008) 3540.
[28] Q.Y. Bi, X.L. Du, Y.M. Liu, Y. Cao, H.Y. He, K.N. Fan, J. Am. Chem. Soc. 134 (2012) 8926.
[29] K. Tedsree, T. Li, S. Jones, C.W.A. Chan, K.M.K. Yu, P.A.J. Bagot, E.A. Marquis, G.D.W. Smith, S.C.E. Tsang, Nat. Nanotech. 6 (2011) 302.
[30] Z.L. Wang, J.M. Yan, H.L. Wang, Y. Ping, Q. Jiang, J. Mater. Chem. A 1 (2013) 12721.
[31] Z.L. Wang, J.M. Yan, Y. Ping, H.L. Wang, W.T. Zheng, Q. Jiang, Angew. Chem. Int. Ed. 52 (2013) 4406.
[32] Z.L. Wang, H.L. Wang, J.M. Yan, Y. Ping, S.J. Li, Q. Jiang, Chem. Commun. 50 (2014) 2732.
[33] Ö. Metin, X. Sun, S. Sun, Nanoscale 5 (2013) 910.
[34] H. Zhang, Ö. Metin, D. Su, S. Sun, Angew. Chem. Int. Ed. 52 (2013) 3681.
[35] Y. Karatas, A. Bulut, M. Yurderi, I.E. Ertas, O. Alal, M. Gulcan, M. Celebi, H. Kivrak, M. Kaya, M. Zahmakiran, Appl. Catal. B: Environ. 180 (2016) 586.
[36] A. Bulut, M. Yurderi, Y. Karataş, Z. Say, H. Kivrak, M. Kaya, M. Gulcan, E. Ozensoy, M. Zahmakiran, ACS Catal. 5 (2015) 6099–6110.
[37] M. Yurderi, A. Bulut, N. Caner, M. Çelebi, M. Kaya, M. Zahmakiran, Chem. Commun. 51 (2015) 11417–11420.
[38] M. Yurderi, A. Bulut, M. Zahmakiran, M. Kaya, Appl. Catal. B: Environ. 160 (2014) 514.
[39] A. Bulut, M. Yurderi, Y. Karatas, M. Zahmakiran, H. Kivrak, M. Gulcan, M. Kaya, Appl. Catal. B Environ. 164 (2015) 324.
[40] J.-M. Yan, Z.-L. Wang, L. Gu, S.-J. Li, H.-L. Wang, W.-T. Zheng, Q. Jiang, Adv. Energy Mater. (2015) 1500107.
[41] X. Gu, Z.-H. Lu, H.-L. Jiang, T. Akita, Q.J. Xu, Am. Chem. Soc. 133 (2011) 11822.
[42] B. Loges, A. Boddien, H. Jınge, M. Beller, Angew. Chem. Int. Ed. 47 (2008) 3962.
[43] E.A. Bielinski, P.O. Lagaditis, Y. Zhang, B.Q. Mercado, C. Würtele, W.H. Bernskoetter, N. Hazari, S. Schneider, J. Am. Chem. Soc. 136 (2014) 10234.
[44] W. Chen, J. Kim, L.-P. Xu, S. Sun, S.J. Chen, Phys. Chem. C 111 (2007) 13452.
[45] K. Jiang, W.B. Cai, Appl. Catal. B 147 (2014) 185–192.
[46] N. Wu, L. Fu, M. Su, M. Aslam, K.C. Wong, V.P. Dravid, Nano Lett. 4 (2004) 383.
[47] H.L. Liu, S. Yoon, S.L. Cooper, G. Cao, J.E. Crow, Phys. Rev. B 60 (1999) 6980.
[48] W.B. Jensen, J. Chem. Ed. 73 (1996) 11.
[49] M. Wawrzyniak, M. Mackowski, Z. Sniadecki, B. Idzikowski, J. Martinek, Acta Phys. Polon. A 118 (2010) 375.
[50] H.S. Belson, J. Appl. Phys. 37 (1996) 1348.
[51] R. Ferrando, J. Jellinek, R.L. Johnston, Chem. Rev. 108 (2008) 845.

[52] J.S. Yoo, F.A. Pedersen, J.K. Nørskov, F. Studt, ACS Catal. 4 (2014) 1226.
[53] J.A. Herron, J. Scaranto, P. Ferrin, S. Li, M. Mavrikakis, ACS Catal. 4 (2014) 4434.
[54] W.E. Kaden, T. Wu, W.A. Kunkel, S.L. Anderson, Science 326 (2009) 826.
[55] J.E. Hutchison, G.H. Woehrie, S. Özkar, R.G. Finke, Turkish J. Chem. 30 (2006) 1.
[56] R. Ferrando, J. Jellinek, R.L. Johnston, Chem. Rev. 108 (2008) 845.
[57] S. Dai, Y. Wu, T. Sakai, Z. Du, H. Sakai, M. Abe, Nanoscale Res. Lett. 5 (2010) 1829.
[58] J. Legrand, C. Petit, D. Bazin, M.P. Pileni, Appl. Surf. Sci. 164 (2000) 186.
[59] N. Su, X. Chen, Y. Ren, B. Yue, H. Wang, W. Cai, H. He, Chem. Commun. 51 (2015) 7195.
[60] C. Yang, A.K. Manocchi, B. Lee, H. Yi, App. Catal. B: Environ. 93 (2010) 282.
[61] J. Cai, H. Huang, B. Huang, S. Zheng, Y. Guo, Int. J. Hyd. Energy 39 (2014) 798.
[62] W. Zhou, J.Y. Lee, Electrochem. Commun. 9 (2007) 1725.
[63] P. Waszczuk, T.M. Barnard, C. Rice, R.I. Masel, A. Wieckowski, Electrochem. Commun. 4 (2002) 599.
[64] N.A. Ray, R.P. Van Duyne, P.C. Stair, J. Phys. Chem. C 116 (2012) 7748.
[65] J. Lu, J.W. Elam, P.C. Stair, Acc. Chem. Res. 46 (2013) 1806.
[66] K. Mori, M. Dojo, H. Yamashita, ACS Catal. 3 (2013) 1114.
[67] M. Yadav, T. Akita, N. Tsumori, Q. Xu, J. Mater. Chem. 22 (2012) 12582.
[68] X. Gu, Z.-H. Lu, H.-L. Jiang, T. Akita, Q. Xu, J. Am. Chem. Soc. 133 (2011) 11822.
[69] M. Yadav, A.K. Singh, N. Tsumori, Q. Xu, J. Mater. Chem. 22 (2012) 19146.
[70] X. Zhou, Y. Huang, W. Xing, C. Liu, J. Liao, T. Lu, Chem. Commun. 39 (2008) 3540.
[71] Y. Huang, X. Zhou, M. Yin, C. Liu, W. Xing, Chem. Mater. 22 (2010) 5122.
[72] Y.-L. Qin, J. Wang, F.-Z. Meng, L.-M. Wanga, X.-B. Zhang, Chem. Commun. 49 (2013) 10028.
[73] S. Ek, E.I. Iiskola, L. Niinisto, J. Vaittinen, T.T. Pakkanen, J. Keranen, A. Auroux, Langmuir 19 (2003) 1.